ELSEVIER

Catalysis Today 28 (1996) 391–403

CATALYSIS TODAY

Transition metal/fluorite-type oxides as active catalysts for reduction of sulfur dioxide to elemental sulfur by carbon monoxide

Wei Liu [a,1], Cyrus Wadia [b], Maria Flytzani-Stephanopoulos [b,*]

[a] *Department of Chemical Engineering, Massachusetts Institute of Technology, Cambridge, MA 02139, USA*
[b] *Department of Chemical Engineering, Tufts University, Medford, MA 02155, USA*

Abstract

Reduction of SO_2 by CO to elemental sulfur on fluorite oxide and transition metal/fluorite oxide composite catalysts is discussed within the redox framework. The oxygen vacancies on the fluorite oxide are active catalyst sites and their creation is a key step to initiate the redox reaction. Transition metal/fluorite oxide composites demonstrate a strong synergism for the reaction. A reduction kinetics study of the copper/ceria system as a model composite catalyst has found that surface oxygen is highly active but its activity is inhibited by SO_2 adsorption. The TPR profile of the copper/ceria catalyst shows a significantly lower reduction peak than the individual components.

1. Introduction

Sulfur dioxide is a precursor to acid rain and a serious health hazard. A main source of SO_2 is coal-fired power plant exhaust gas streams. Flue gas desulfurization (FGD) is currently accomplished by non-catalytic processes such as wet or dry scrubbing. These commercial processes generate large amounts of solid waste to be disposed of and also involve high operating cost. Recent development efforts have emphasized dry regenerative processes with simultaneous NOx removal involving no throwaway waste. In a typical dry regenerative FGD process, sulfur dioxide in the flue gas stream reacts with a metal oxide sorbent to form metal sulfate and then the saturated oxide sorbent is regenerated by a reducing gas stream to the oxide form for cyclic operation. A gas stream containing SO_2 is released by the regeneration. Treatment of this regeneration off-gas is integrally related to the regenerative FGD process and will be a determining factor for the commercial viability of any regenerative FGD.

Direct reduction of sulfur dioxide in the regenerator off-gas to elemental sulfur is an attractive approach, because it involves a simplified flow sheet and produces a saleable product. Development of a highly efficient, single-stage catalytic converter for this purpose will significantly benefit the commercialization of the new generation FGD processes. Most of previous

* Corresponding author.
[1] Current address: Mail Station H-2, Amoco Oil Company, Amoco Research Center, P.O.Box 3011, Naperville, IL 60566.

PII S0920-5861(96)00248-9

studies of reduction of sulfur dioxide to elemental sulfur examined carbon monoxide as the reductant. A variety of catalyst materials have been studied, including transition metals and mixed oxides. The perovskite-type mixed oxides have received a lot of attention. A class of ABO_3-type mixed oxides consisting of alkaline earth, rare earth, and transition metal elements were disclosed in a patent by Whelan [1]. Happel and co-workers [2,3] proposed a redox reaction mechanism involving surface oxygen/oxygen vacancy participation for La–Ti–O perovskite oxide catalysts. The SO_2 reaction with CO over $Sr_xLa_{1-x}CoO_3$ perovskite catalysts was also discussed by Hibbert and Campbell within the redox framework [4,5]. Perovskite oxides, such as $LaCoO_3$, have both excellent electronic conductivity and oxygen ion mobility [6]. The previous studies suggest that the oxygen vacancy or mobility may be an important catalyst property for SO_2 reduction by CO. However, perovskite oxides are not stable under the reaction conditions and decompose into metal sulfide and oxysulfide. Recently, a COS reaction intermediate mechanism was proposed for this type of catalysts [7], that is, CO reacts with metal sulfides to form COS and then COS reduces SO_2 to elemental sulfur. We have found that cerium oxide undoped or doped with rare earth oxides is a highly active and stable catalyst for SO_2 reduction by CO [8,9] and zirconium oxide also has comparable activity to cerium oxide [10,11]. Cerium and zirconium oxide are fluorite oxides well known for their high oxygen vacancy and mobility properties [12]. These refractory materials keep their crystal structure in the highly reactive sulfur atmosphere. In addition, the catalytic activity and resistance to impurities such as water vapor of the fluorite oxide catalysts can be significantly enhanced by addition of small amounts of transition metals, such as Cu, Ni, Co, etc. [10,11]. The resulting transition metal/fluorite oxide composite catalysts have superior performance to the other catalysts disclosed in the literature.

In this paper we discuss SO_2 reduction by CO over the fluorite oxides and transition metal/fluorite oxides catalysts along the lines of oxygen mobility, catalyst reducibility, and interaction of the transition metal/fluorite oxide. Among various catalyst compositions we chose Cu–Ce(D)O_2 (D = dopant) as a model system, while the other catalysts were briefly examined.

2. Experimental

2.1. Catalyst preparation and characterization

Low purity cerium nitrate containing about 1.5 wt.-% La was typically used for catalyst synthesis. The cerium from this precursor is designated as Ce(La) in the catalyst formula throughout the paper. High purity cerium nitrate (99.9%, Aldrich) was used to prepare the catalysts containing different dopant ions (Sr, Sc, La, Gd). Pure cerium oxide of reasonable surface area (ca. 26 m^2/g) and mesopore size (ca. 20 nm) was made from direct thermal decomposition of cerium acetate (Aldrich) for 4 h at 750°C. γ-Al_2O_3 support was supplied by LaRoche. Cerium oxide doped with alkaline earth and rare earth oxide, Ce(D)O_2, was prepared by a complexation technique with citric acid [9]. This method yielded high pore volume and a large fraction of macropores (> 1 μm). However, the resulting catalyst was bulky and had a packing density of typically 0.1 g/cc so that a large reactor volume was required. The transition metal/fluorite oxide composite catalysts were mainly synthesized by a conventional coprecipitation method and typically calcined for 4 h 650°C. The supported catalysts were prepared by the conventional wet impregnation method using aqueous salt solutions of the metals. The impregnated samples were dried for a few days at room temperature and then heated in air for 4 h at 650°C. Further details of the catalyst preparation procedure are given in [11].

Bulk CeO_2 is a very stable compound. In

contrast, no air-stable, non-stoichiometric cerium oxide has ever been synthesized, because reduced CeO_2 is immediately re-oxidized when exposed to air or moisture. Non-stoichiometric cerium oxide, CeO_{2-x}, studied in this work was synthesized by Tschope in an ultra-high vacuum (UHV) apparatus by magnetron sputtering of a metallic target and controlled oxidation [13,14]. Due to high materials and operation costs, only three catalysts were prepared by this method. They are pure CeO_{2-x}, 10 at.% La-doped CeO_{2-x}, and 15 at.% Cu-doped CeO_{2-x}. The major finding was that non-stoichiometric cerium oxide prepared by this method is stable at atmospheric conditions and can keep certain non-stoichiometry properties even after air calcination at high temperatures. Catalytic activities of the non-stoichiometric cerium oxide catalysts are reported in this paper for comparison with the bulk catalyst.

For bulk composition analysis, the catalyst powder was dissolved in concentrated hydrofluoric acid solution and then diluted by de-ionized water. The resulting solution was analyzed by inductively coupled plasma (ICP) atomic emission spectrometry (Perkin Elmer Plasma 40). The catalyst surface composition was analyzed by X-ray Photoelectron Spectroscopy (XPS). The total BET surface area was routinely measured by single-point N_2 adsorption and desorption on a Micromeritics 2000 instrument. Selected catalysts were analyzed on a Micromeritics ASAP 2000 apparatus by multipoint BET surface area and pore size distribution measurements. Powder X-ray diffraction (XRD) analyses were performed on a Rigaku 300 X-ray Diffractometer with a Rotating Anode Generators monochromatic detector, and a DEC VAX Station II computer for complete control and data recording as well as for data processing. Copper $K\alpha 1$ radiation was used with power settings of 50 kV and 200 mA. For crystal phase survey, typical operation parameters were divergence slit 1°, scattering slit 1°, receiving slit 0.3°, and scan rate 1 to 10°/min with 0.02° data interval. XPS analyses were performed on a Perkin Elmer 5100 system with 2 mm spatial resolution. The measurements were carried out at room temperature and without any sample pretreatment. A Mg $K\alpha$ X-ray source was used with an incident energy of 1253.6 eV. The X-ray generator power was typically set at 15 kV and 20 mA. A C1s peak was found in all measurements resulting from ambient hydrocarbons in the sample, and was used as an internal standard. Therefore, all binding energies were adjusted relative to C1s at 284.6 eV.

2.2. Apparatus

Catalyst activity was tested in a laboratory-scale, quartz tube packed bed reactor with a porous quartz frit placed at the middle for supporting the catalyst. A 0.6 cm I.D × 50 cm long reactor was used in regular catalyst tests, while a 1.0 cm I.D. reactor was used for high volume catalyst loading. The reactor tube was heated by a Lindberg furnace. The reaction temperature was monitored by a quartz tube-sheathed K-type thermocouple placed at the top of the packed bed and controlled by a Wizard temperature controller. The reacting gases, all certified calibration gas mixtures with helium (Matheson), were measured with mass flow controllers and mixed prior to the reactor inlet. The resulting gas mixture flowed downward through the packed bed. Water vapor was introduced with helium bubbling through a heated water bath. The experiments were carried out at nearly atmospheric pressure. Elemental sulfur produced by the SO_2 reduction was condensed out in a cold trap installed at the outlet of the reactor. A filter was installed at the entrance of the GC gas sample loop to protect it against entrained particles. The product gas was analyzed by a HP 5880A Gas Chromatograph (GC) with a Thermal Conductivity Detector (TCD). A 1/4″ O.D. × 6′ long packed column of Chromosil 310 (from SUPELCO) operated at 60°C provided baseline separation of CO, CO_2, COS, H_2S, CS_2, and SO_2.

Some quantities referred in the text,

$[CO]/[SO_2]$ molar ratio (R_{CO}), sulfur yield (Y-sulfur), and SO_2 conversion (X-SO_2) are defined as follows:

$$R_{CO} = [CO]_{inlet}/[SO_2]_{inlet} \quad (1)$$

$$Y - \text{sulfur} = [\text{Sulfur}]_{outlet}/[SO_2]_{inlet} \quad (2)$$

$$X - SO_2 = ([SO_2]_{inlet} - [SO_2]_{outlet})/[SO_2]_{inlet} \quad (3)$$

where $[CO]_{inlet}$ and $[SO_2]_{inlet}$ are molar fractions of CO and SO_2 in the feed gas; $[\text{Sulfur}]_{outlet}$ and $[SO_2]_{outlet}$ are molar fractions of elemental sulfur and SO_2 in the exit gas.

The reducibility of the catalyst was studied in a Cahn TG 121 thermogravimetric analyzer (TGA) coupled with a MKS quadrupole mass spectrometer attached for gas analysis. For the temperature programmed reduction (TPR) experiments, a few mg of catalyst were loaded into a quartz pan. After the system was stabilized in pure nitrogen at 50°C, the reducing gas (CO or H_2) was introduced and the temperature was raised at a rate of 10°C/min to 850°C. Data were acquired every four seconds. The resulting TPR profile was corrected with the blank test. For isothermal reduction kinetics experiments, the temperature was raised to a given value in N_2 and stabilized. Reducing gas was then introduced and data were acquired every one second. A high flow rate, 600 sccm, was used in the TGA experiments so that mass transfer limitation was eliminated. The reduction rate is defined as follows:

$$R = -\frac{\Delta W}{W_0 \Delta t} \times 100\% \quad (4)$$

where ΔW and W_0 denote the weight change in a time interval Δt and initial weight, respectively.

3. Results and discussion

3.1. Catalytic properties of fluorite-type oxides

Fig. 1 shows the crystal structure of fluorite oxides. The fluorite oxide has a face-centered cubic lattice in which the large tetravalent (+4) ions, such as Ce^{+4}, Zr^{+4}, Th^{+4}, etc., have an eight-coordination of oxygen ions. A unit cell contains four cations occupying four opposite corners. Oxygen vacancies are created when the tetravalent lattice cations are replaced by divalent or trivalent dopant (impurity) ions. Alkaline earth and rare earth oxides, such as MgO, La_2O_3, Y_2O_3, etc., are common dopant oxides. These oxides generally have substantial solubility in fluorite oxides ranging from 2 to 100% [15]. In contrast, transition metal oxides have little solubility in fluorite oxides. High oxygen vacancy concentration and oxygen mobility are well-known properties of fluorite oxides. These materials are extensively studied as oxygen ion conductors [12]. In the catalysis field, they have been used as a promoter in automotive three-way catalysts [16], but usually they are not considered active catalyst components.

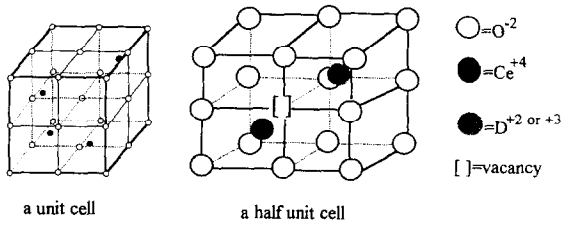

Fig. 1. Lattice structure of a fluorite-type oxide.

Catalytic behavior of fluorite oxides for SO_2 reduction by CO is illustrated in Fig. 2. The

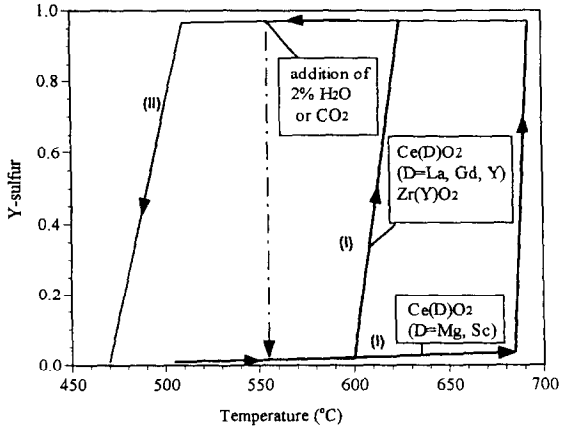

Fig. 2. Catalytic performance of fluorite oxides for SO_2 reduction by CO (1% SO_2, 2% CO, 0.030 g·s/cm^3 (STP); (I) ascending temperature; (II) descending temperature).

branch I in Fig. 2 is the light-off curve showing the temperature at which reaction starts. For these tests, we started with the fresh catalyst without any pretreatment by a reducing agent, raised the reaction temperature from 500 to 700°C in 50°C-steps, and held each temperature constant for about half an hour until complete reaction occurred. We found that the reaction was lighted off in the neighborhood of 600°C over all the La-doped ceria catalysts, independent of dopant content and the amount of catalyst used. The yttria-doped zirconia has a similar light-off temperature. However, a higher light-off temperature ($\sim$ 690°C) was measured for Mg and Sc-doped ceria catalysts. The branch II in Fig. 2 represents the fall-off behavior. This curve was obtained by lowering the reaction temperature in 50°C-steps until the reaction was quenched. The fall-off temperatures for the fluorite oxide catalysts were in the neighborhood of 500°C. The light-off and fall-off temperatures could not be lowered by increasing the contact time beyond a certain value, ca. 0.02 g · s/cc(STP). Also, the light-off temperature could not be lowered by increasing the dopant level. These temperatures appear to be associated with the intrinsic properties of the fluorite oxide.

With the stoichiometric feed gas ($R_{CO} = 2$) only small amounts of COS (less than 5%) were produced. Therefore, the sulfur yield in Fig. 2 basically represents the SO_2 conversion. The fluorite oxides showed high stability and selectivity to elemental sulfur. Only the fluorite structure was identified by XRD for both fresh and used catalysts. However, the fluorite oxide catalysts were very sensitive to impurity gases. The catalyst completely lost its activity at 550°C when 2% H_2O or CO_2 was introduced into the reacting gas stream. Resistance to water vapor could not be improved by using alkaline earth and rare earth oxide dopants. It was observed that the catalyst could be activated by either pre-reduction or by reaction at high temperatures; a partially reduced surface comprised the working catalyst. The surface state of cerium oxide was easily observed during the experiment, because bulk ceria appeared pale yellow, while a reduced surface had a dark blue color.

The catalytic behavior of fluorite oxides is explained within a redox reaction framework consisting of reduction of the catalyst surface by CO and oxidation of the reduced catalyst surface by SO_2.

$$\text{cat-O} + \text{CO} \rightarrow \text{cat-[ ]} + \text{CO}_2 \quad (5)$$

$$\text{cat-[ ]} + \text{SO}_2 \rightarrow \text{cat-O} + \text{SO} \quad (6)$$

$$\text{cat-[ ]} + \text{SO} \rightarrow \text{cat-O} + \text{S} \quad (7)$$

An oxygen vacancy is created as a surface capping oxygen is removed by CO. Then, SO_2 donates its oxygen to the vacancy to form SO. The SO is mobile on the surface until it finds another vacancy to donate its oxygen or a vacancy may migrate to a neighboring site to accept its oxygen. High oxygen ion mobility in the catalyst will facilitate the oxygen transfer from one site to another on the surface or from the bulk to the surface. However, the oxygen vacancy can be taken up by other oxidizing agents such as H_2O. The stronger these impurity oxygen atoms attach to the vacancy, the more severe their inhibition effect. The activation tests proved that the creation of oxygen vacancies on the catalyst surface is a key step to start the reaction.

It is oxygen vacancies as active catalytic sites that make fluorite oxide active for SO_2 reduction by CO. It is known that the oxygen vacancy concentration of fluorite oxides can be enhanced by using alkaline earth and rare earth oxide dopants. However, the surface oxygen vacancies are always capped by oxygen atoms from ambient oxygen. Therefore, the capping oxygen has to be removed to activate the catalyst. The oxygen vacancy and the dopant ion are energetically associated ion pairs. The associated energy is a strong function of the type of dopant ion and dopant content [17].

Our previous research [9] indicates that the specific catalytic activity of cerium oxide can be improved by using small amounts (a few atomic percent) of Y or La dopant. However, alkaline

earth and rare earth dopants are not effective to lower the reduction temperature of the surface capping oxygen and change the surface properties of the fluorite oxide. Water vapor not only takes up the oxygen vacancy as we mentioned above but also inhibits CO adsorption on cerium oxide according to recent FTIR studies [18,19]. In conclusion, the oxygen vacancy property of fluorite oxide is relevant for catalytic reduction of SO_2 by CO, but not sufficient for an active and stable catalyst that is resistant to water vapor poisoning.

3.2. Transition metal / fluorite oxide catalysts

Significant improvement of fluorite oxide catalysts in both activity and tolerance to water vapor was achieved by the addition of small amounts of transition metals, such as Cu, Ni, Co, Pt [11]. Typical results of the transition metal/fluorite oxide composite catalysts are illustrated in Fig. 3. The light-off temperatures over the Cu–Ce(La)–O and Cu–Zr(Y)–O catalysts were lowered to ca. 500°C from ca. 600°C, while a conventional alumina-supported Cu catalyst shows a light-off temperature of about 550°C. A synergistic effect was clearly demonstrated for the Cu-fluorite oxides systems. It is interesting that the copper content in the Cu–Ce(La)–O catalysts did not affect the light-off temperature and sulfur yield under the same reaction conditions. Separate studies show that water vapor does not poison the catalyst but the sulfur yield decreased a little as a result of promotion of the water–gas-shift reaction and production of H_2S [11]. For example, no catalyst deactivation was observed during a 34-h run with the $Cu_{0.15}[Ce(La)]_{0.85}O_x$ catalyst at 470°C in the presence of 2% H_2O.

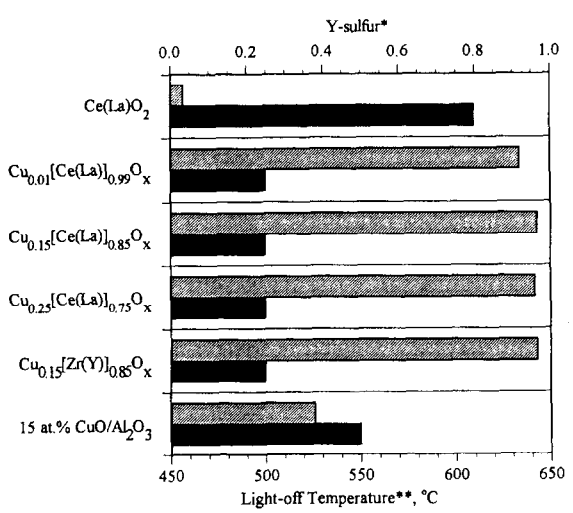

Fig. 3. Light-off temperature and sulfur yield of SO_2 reduction by CO over various oxide composite catalysts (1% SO_2, 2% CO, 0.09 g·s/cm^3 (STP)). Shaded bars = sulfur yield (Y-sulfur); black bars = light-off temperature. * Sulfur yield at 470°C after catalyst was activated. ** Light-off temperature at which 90% conversion occurred.

Transition metals themselves are active catalysts for SO_2 reduction by CO [20–22]. However, transition metals are typically sulfided at the reaction conditions. A reaction mechanism involving COS intermediate was proposed for such catalysts [21,22]. Based on this theory, COS is formed by reaction of CO with metal sulfide as expressed by reaction (8) and then, COS reduces SO_2 to produce elemental sulfur through reaction (9).

$$MS_x + CO \rightarrow MS_{x-1} + COS \quad (8)$$

$$2COS + SO_2 \rightarrow 3/x\, S_x + 2CO_2 \quad (9)$$

However, the present composite catalysts exhibit unique catalytic properties to either fluorite oxide or transition metal alone. The composite catalyst has higher activity than each of the individual component. No COS intermediate was detected in extensive kinetic studies of the composite catalyst in both a fixed bed microreactor and TGA-MS apparatus [23]. COS was produced over the composite catalyst as a secondary product only when more than the stoichiometric amount of CO was used. In other words, COS was formed by the reaction of product sulfur with CO. This is illustrated in Fig. 4 which shows the variation of SO_2 conversion and sulfur yield with R_{CO} under constant reaction temperature (470°C) and constant contact time (0.0113 g·s/cc(STP)). It can be seen that under such a short contact time the

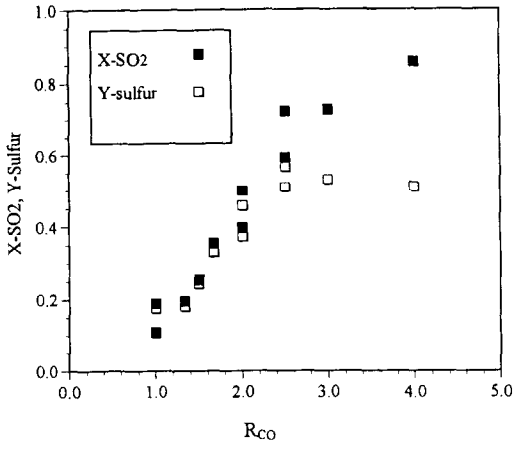

Fig. 4. SO_2 conversion and sulfur yield as a function of R_{CO} (0.0113 g·s/cm^3 (STP), 470°C).

converted SO_2 is almost the same as the sulfur yield at low R_{CO}. The difference between SO_2 conversion and sulfur yield is COS yield. The COS yield increased with R_{CO}.

The fluorite oxide structure is stable during the reaction in contrast to what has been reported in the literature for perovskite structures [5,7]. The fluorite oxide is in excess and serves as the backbone of the composite catalyst. Transition metals or oxides are dispersed in the fluorite oxide as additives and in turn modify the properties of the fluorite oxide. Therefore, cerium oxide in the Cu–Ce–O composite is not simply a support material for copper dispersion. There is a strong interaction between these two kinds of materials. Extensive characterization results of the fresh Cu–Ce–O catalyst by XPS, XRD, and STEM/EDX were recently reported elsewhere [24,25]. For this class of composite catalysts prepared by 650°C air-calcination, no CuO phase was detected at copper contents lower than 15 at.%. Copper was distributed in the cerium oxide in the form of isolated ions, clusters, and bulk CuO particles. The copper clusters were found in all the Cu–Ce–O catalysts, while the CuO content increased with the bulk copper content. Cu^{+1} species were observed by XPS on the Cu–Ce–O catalyst and are considered a result of the interaction of copper clusters and cerium oxide lattice. However, sulfur compounds are so reactive that the catalyst composition often changed after the reaction. XRD and STEM analyses of the spent catalysts [23] identified that the cerium oxide matrix was not attacked by sulfur compounds and still held its fluorite crystal structure, while bulk CuO was completely converted into copper sulfide crystals, and copper and sulfur were extensively distributed on the cerium oxide matrix.

The surface compositions of two Cu–Ce(La)–O catalysts after reaction are shown in Table 1. More copper was measured by XPS than the nominal bulk value, indicating surface enrichment in copper. Significant amounts of sulfur were found in all the catalysts. The oxygen content is much higher than the nominal values calculated by assuming Cu as CuO and Ce as CeO_2. These large amounts of excess oxygen suggest that sulfur mainly exists as sulfates. Generally, more oxygen and sulfur were found with the catalysts in the inactive state than in the active state. The surface states of these elements were determined by the binding energies of Ce3d, Cu2p, S2p and O1s core electrons [11,23]. Cerium existed as cerium sul-

Table 1
Surface compositions of used Cu–Ce(La)–O catalysts [a]

Element	$Cu_{0.02}[Ce(La)]_{0.98}O_x$		$Cu_{0.15}[Ce(La)]_{0.85}O_x$	
	6 h at 440°C [b]	two days [c]	2 h at 433°C [d]	2 h at 510°C [e]
Ce	23.2	25.2	9.9	23.1
Cu	2.6	5.3	7.3	9.2
S	5.9	5.6	13.7	6.8
O	68.2	63.9	69.1	60.8
$O_{theoretical}$ [f]	49.0	55.7	27.1	55.4
$O_{difference}$ [g]	19.2	8.2	42	5.4

[a] Reaction gas: 1% SO_2, 2% CO/He. Contact time: W/F = 0.09 g·s/cm^3 (STP).
[b] Catalyst was completely deactivated at this temperature.
[c] Catalyst was tested in the active state for two days.
[d] Catalyst was completely deactivated.
[e] Catalyst was fully activated at this temperature and complete SO_2 conversion occurred.
[f] Oxygen content calculated on the basis of CuO and CeO_2.
[g] Difference in oxygen content between the measured and calculated values.

fate and cerium oxide. Copper existed as copper oxide, sulfide, and sulfate. Oxygen existed as metal oxide and sulfate. Sulfur existed as sulfate and sulfide. The major conclusion from the XPS analyses is that a working Cu–Ce(La)–O catalyst comprised partially sulfided copper and partially sulfated cerium, while the cerium oxide in a deactivated catalyst was fully capped by sulfate.

The catalytic properties of the Cu–Ce(La)–O catalyst can be understood on the basis of the proposed redox reaction scheme. Surface reduction by CO is still the key step to initiate the reaction. However, under the reaction conditions, SO_2 and CO would compete for the surface oxygen. Reaction of CO with the surface capping oxygen produces CO_2 and an oxygen vacancy (Eq. (5)), while reaction of SO_2 with the surface oxygen forms sulfate:

$$SO_2 + 2O\text{-cat} \xrightarrow{\text{strong}} SO_4\text{-cat} \quad (10)$$

The sulfate is a strongly bound surface species and its formation tends to terminate the redox reaction. Therefore, the rate of the surface oxygen reduction by CO has to be greater than that of sulfation by SO_2 if the fresh catalyst is activated in the reacting gas mixture. After the surface oxygen and sulfate are removed, the redox reaction is initiated and the reaction can be operated at lower temperatures. We propose that copper and cerium oxide play different roles in the redox reaction. Cerium oxide comprises the matrix of the catalyst and provides the oxygen/oxygen vacancy sources, while copper as an additive promotes the reducibility of cerium oxide and provides the surface sites for CO adsorption. This reaction model is depicted in Fig. 5. The catalyst characterization results

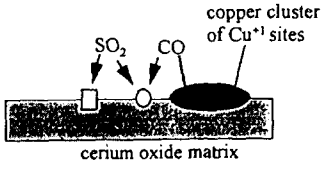

Fig. 5. Synergistic reaction model for SO_2 reduction by CO over Cu–CeO_2 composite catalyst. □ oxygen vacancy, ○ surface capping oxygen.

have shown that Cu^{+1} species tend to be stabilized by the interaction of the copper clusters and the cerium oxide lattice. It is known that Cu^{+1} sites are strong sites for CO chemisorption. The promotion effect of copper on the surface reduction is discussed below in Section 3.4.

The Cu^{+1} species were observed by XPS on the fresh catalyst. However, the catalyst surface became complex in the CO + SO_2 reacting atmosphere. CuO particles formed copper sulfide crystals that have low surface area and contributed little to the catalytic activity. It is not known at the present time how copper ions and clusters in the cerium oxide matrix are affected by sulfur compounds. According to a recent study by Badley et al. [26] of SO_2 and CO adsorption on Cu/Al_2O_3, SO_2 can block CO adsorption on Cu^{+2} sites but not on Cu^{+1} sites, while the pre-adsorption of CO does not prevent SO_2 adsorption. Therefore, copper in the Cu–Ce(La)–O composite catalyst may still provide strong sites such as Cu^{+1} for CO adsorption even in the presence of sulfur compounds and water vapor. However, the cerium oxide surface can be completely capped by sulfate when the composite catalyst is exposed to SO_2 gas at temperatures below or around 500°C. The sulfated cerium oxide surface would have no oxygen vacancy sites to catalyze the reaction. The proposed active catalyst configuration suggests that only small amounts of copper are needed to achieve the synergism. Given the fact that copper oxide is not miscible with cerium oxide, use of excess copper only generates more bulk CuO particles that are converted to copper sulfide at the reaction conditions. This explains why the catalyst light-off temperature and activity were not much affected by copper content.

3.3. SO_2 reduction by CO over non-stoichiometric cerium oxide catalysts

The above results and discussion provide evidence that active sites for SO_2 reduction by CO are on the reduced cerium oxide surface. How-

ever, bulk reduction of cerium oxide only occurs at 700 to 800°C and even surface reduction of the capping oxygen still requires a temperature around 500°C [27].

$$CeO_2 + \delta CO(\text{or}\,H_2) \rightarrow CeO_{2-\delta} + \delta CO_2(\text{or}\,H_2O) \quad (11)$$

Air-stable, reduced cerium oxide or non-stoichiometric cerium oxide has never been synthesized, since the reduced catalyst is immediately oxidized at ambient conditions. Stable, non-stoichiometric cerium oxides in the present study have been synthesized in nanocrystalline form [13,14]. These materials contain large concentrations of lattice defects such as oxygen vacancies and free electrons. The general catalytic oxidation properties of the non-stoichiometric cerium oxide materials were reported in Ref. [14]. The light-off and fall-off behavior of three such catalysts, i.e. CeO_{2-x}, 10 at.% La-doped CeO_{2-x}, and 15 at.% Cu-doped CeO_{2-x}, for SO_2 reduction by CO were evaluated in the same manner as the bulk catalysts prepared by coprecipitation. The major results are summarized in Fig. 6.

The light-off temperature on the pure CeO_{2-x} catalyst was decreased by ca. 100°C compared to the bulk CeO_2. A small hysteresis effect was observed with the CeO_{2-x} and negligible hysteresis was observed with the La-doped CeO_{2-x}. The undoped and La-doped CeO_{2-x} catalysts showed even better performance than the bulk $Cu_{0.15}[Ce(La)]_{0.85}O_x$ prepared by coprecipitation. The reduced cerium oxide makes the surface deficient in oxygen so that less surface sulfate is formed. The extensive presence of oxygen vacancies greatly facilitates the catalyst activation. This is further seen by the activation profiles of 15 at.% Cu-doped CeO_{2-x} and bulk $Cu_{0.15}[Ce(La)]_{0.85}O_x$ catalysts shown in Fig. 7. It took about 140 min for SO_2 to reach 70% conversion at 460°C on the bulk $Cu_{0.15}[Ce(La)]_{0.85}O_x$ catalyst without any pretreatment. However, the conversion rose rapidly even at a lower temperature (435°C) over the same catalyst when pre-reduced by CO at 400°C. The activation profile of the as prepared, non-stoichiometric Cu-doped catalyst is close to the CO-reduced catalyst. Thus, a partially reduced cerium oxide surface is vital to starting and sustaining the redox reaction cycle. These results strongly support the present mechanistic model.

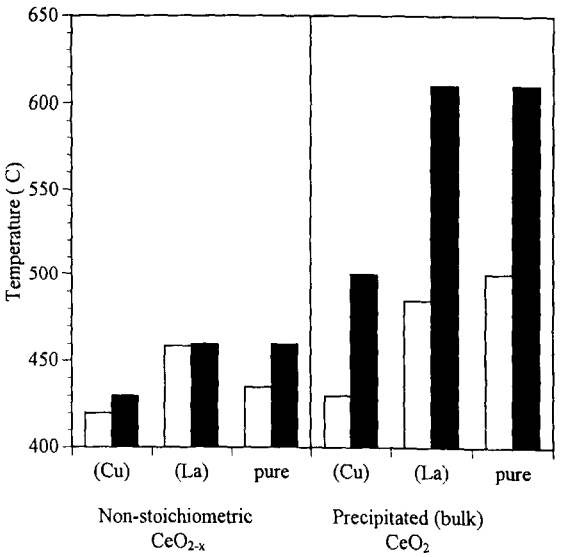

Fig. 6. Light-off (filled bars) and fall-off (open) temperatures of non-stoichiometric and precipitated cerium oxide catalysts for 90% SO_2 reduction by CO (1% SO_2, 2% CO, 0.09 g·s/cm^3 (STP)). (Cu) = 15 at.% Cu-doped, (La) = 10 at.% La-doped.

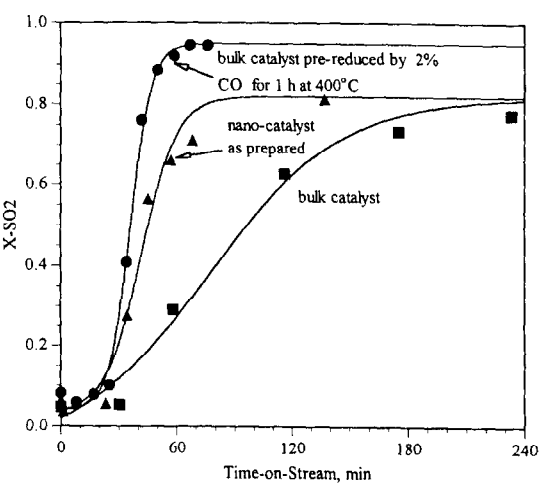

Fig. 7. Activation profiles of the 15 at%. Cu-containing Cu–Ce–O catalysts in the reacting gas mixture (1% SO_2, 2% CO, 0.06 g·s/cm^3 (STP)). Test temperatures: ■ 460°C, ● 435°C, ▲ 450°C.

The S-shaped activation profile is typical for the present catalyst system. An induction period is shown in Fig. 7. This is probably caused by rapid uptake of SO_2. As we will discuss below, the initial SO_2 adsorption rate is much faster than the CO reduction rate. The catalyst surface is immediately covered by SO_2 upon the introduction of reaction gas mixture. As the surface SO_4^{2-} is gradually removed by CO reduction and decomposition itself, clean catalyst surface is exposed. The more clean surface is exposed, the more rapidly the surface reduction proceeds. Therefore, the activation behaves like an autocatalytic process. However, the catalyst activation is a complex process and detailed analysis is beyond the scope of this paper.

3.4. Reducibility of the $Cu_{0.15}[Ce(La)]_{0.85}O_x$ catalyst

The catalyst reducibility is an important attribute for SO_2 reduction by CO based on the above discussion. The reducibility of the Cu–Ce–O system was investigated using the $Cu_{0.15}[Ce(La)]_{0.85}O_x$ material as a model catalyst. Fig. 8 shows a typical temperature-programmed reduction profile of the catalyst in high purity 5% H_2/He that was corrected by the TPR profile of the same catalyst in high purity He alone. The reduction started at ca. 100°C. A peak appeared around 150°C. After 200°C the weight slowly decreased with temperature. Above 500°C the weight loss rapidly increased with temperature. This period is considered as bulk reduction of cerium oxide. This TPR profile demonstrates a remarkable synergism or 'strong interaction' between copper and cerium oxide. According to Yao and Yao [27], the reduction peak of surface capping oxygen on the bulk CeO_2 occurs around 500°C. TPR studies [28,29] of bulk CuO materials found that the reduction peaks typically appeared between 200 to 300°C.

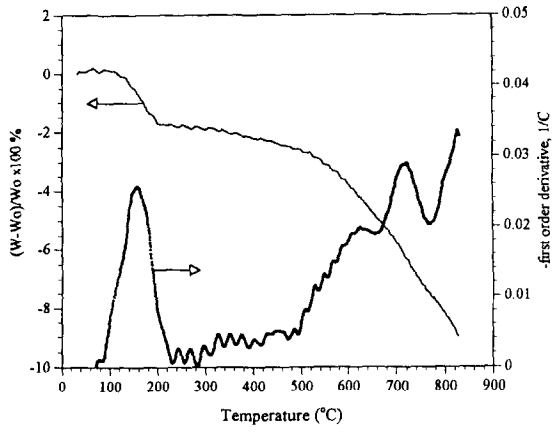

Fig. 8. TPR profile of $Cu_{0.15}[Ce(La)]_{0.85}O_x$ catalyst in 5% H_2 /He.

Very small and broad CuO peaks were identified in the XRD analysis of the $Cu_{0.15}[Ce(La)]_{0.85}O_x$. STEM/EDX analyses of this catalyst found that most part of copper distributed on the cerium oxide matrix as clusters with only a small fraction presented as CuO particles. Apparently, the combination of copper and cerium oxide significantly lowered the catalyst surface reduction temperature compared to either bulk CuO or CeO_2. The weight loss at 300°C was about 2%, while the weight loss from complete reduction of CuO to Cu is 1.57% if all Cu in the composite catalyst is assumed to exist as CuO. The extra weight loss is very likely due to the reduction of surface capping oxygen on the cerium oxide. Interestingly, the TPR profile in Fig. 8 resembles those of precious metal (Pt, Rh)/CeO_2 systems that are model systems for 'strong metal–support interaction' [27,30].

Since CO is a reacting gas in the present study, it would be more relevant to study the reducibility of the Cu–Ce(La)–O catalyst by CO. Fig. 9 shows the reduction profiles of the $Cu_{0.15}[Ce(La)]_{0.85}O_x$ in 0.5% CO/N_2 at different temperatures. Rapid initial reduction followed by a slower reduction branch was observed at temperatures of 200°C or greater. The reduction depth and rate increase with temperature. The reduction curve at 100°C confirmed that the present catalyst can be reduced at much lower temperature than either CuO or CeO_2. The reduction profiles at lower temperatures can be fitted with a first-order equation, while these

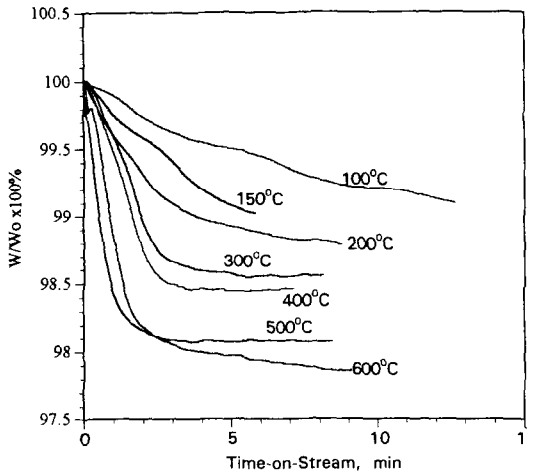

Fig. 9. Reduction profiles of fresh $Cu_{0.15}[Ce(La)]_{0.85}O_x$ catalyst in 0.5% CO/N_2 at different temperatures.

at higher temperatures cannot. Multiple processes involving surface diffusion and bulk diffusion become significant at high temperatures. The reduction extent after 3 min at 500°C began to level off at 98.1%. Therefore, some surface oxygen from cerium oxide was removed. Overall, hydrogen reduction seems more extensive at high temperatures than CO-reduction. It is noted that the present catalyst is a bulk catalyst and a significant amount of copper oxide was embedded in the cerium oxide matrix. Reduction of copper oxide may proceed simultaneously with surface reduction of cerium oxide. Fig. 10 shows

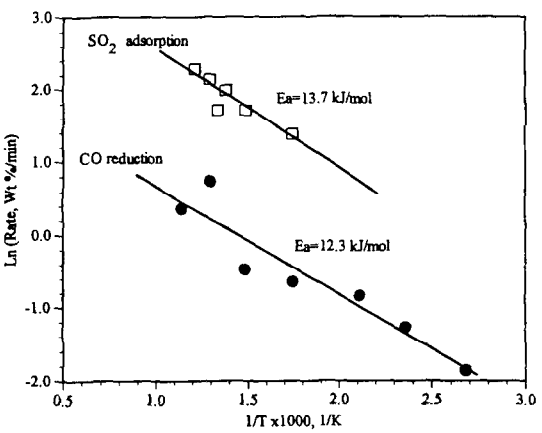

Fig. 10. Arrhenius plots of the initial CO reduction rate of and SO_2 adsorption rate on fresh $Cu_{0.15}[Ce(La)]_{0.85}O_x$ catalyst.

the Arrhenius plot of the initial reduction rates. The data are regressed with a linear equation. The resulting activation energy is only 12.3 kJ/mol. Separate studies show that mass transfer limitation is eliminated at the 600 sccm flow rate used in this work. The activation energy for CO oxidation over this catalyst is 78 kJ/mol [25]. The low activation energy of reduction suggests that these surface oxygen species are highly active.

3.5. SO_2 uptake on the $Cu_{0.15}[Ce(La)]_{0.85}O_x$ catalyst and CO reduction

The above reduction results show that fresh $Cu_{0.15}[Ce(La)]_{0.85}O_x$ catalyst is highly reducible by CO or H_2. However, the activity test results show that a light-off temperature as high as 500°C was needed to start the reaction of SO_2 and CO. At reaction conditions, SO_2 and CO compete for the surface oxygen so that the catalyst reducibility is suppressed. To check this, SO_2 uptake and reduction of sulfated catalyst were studied. In this experiment, the TGA temperature was raised to a given value in pure N_2 and after the system was stabilized, 1% SO_2/N_2 gas was introduced. Although no oxygen was fed, the catalyst showed rapid weight gain upon introduction of SO_2. This indicates that SO_2 reacted with catalyst surface oxygen, because cerium oxide has high oxygen storage capacity. Even in the presence of oxygen, Hedges and Yeh [31] have found that the SO_2 uptake rate on the CeO_2/Al_2O_3 sorbent is independent of P_{O_2}. Following the rapid gain upon introduction of SO_2, the catalyst weight gradually increased with time-on-stream. The Arrhenius plot of the initial SO_2 uptake rate is shown in Fig. 10. The SO_2 uptake rate is much faster than the CO reduction rate. The activation energy is 13.7 kJ/mol. Therefore, the cerium oxide surface is active for sulfate formation.

Reducibility of the sulfated catalyst was studied by exposing the catalyst to 1% SO_2/N_2 for about 10 to 20 min at the reduction temperature prior to introduction of 2% CO/N_2. No appar-

ent reduction was observed below 400°C, as opposed to the significant and rapid reduction of the fresh sample below this temperature. The Arrhenius plot of the initial reduction rate of the sulfated catalyst is shown in Fig. 11. Clearly, two reduction regimes exist. Below 550°C, the reduction rate steeply increases with temperature, resulting in an activation energy of 160 kJ/mol. Above 550°C, the activation energy is very small and comparable to that for fresh catalysts.

Therefore, SO_2 can rapidly react with the surface capping oxygen to form strongly bound surface sulfate. In the presence of CO, the sulfate may be reduced back to SO_2 but the reduction is slow and has a high activation energy. At high temperatures (ca. 550°C) the desorption of the adsorbed SO_2 becomes significant in the absence of gaseous SO_2 that the catalyst surface reduction by CO readily occurs.

$$SO_4\text{-cat} + 2CO \overset{\text{slow}}{\rightarrow} SO_2 + 2CO_2 + 2[\,]\text{-cat} \quad (12)$$

$$SO_4\text{-cat} \overset{\text{high T}}{\rightarrow} SO_2 + 2O\text{-cat} \quad (13)$$

Under the reaction conditions, SO_2 will immediately capture the surface oxygen when the catalyst is exposed to the reacting gas, SO_2 and CO. Therefore, a high reduction temperature is required for CO to keep the surface free of sulfate. As catalyst surface vacancies are created by CO, the reaction temperature can be decreased. An apparent reduction of the sulfated surface needs a temperature around 450 to 500°C which is comparable to the light-off temperature.

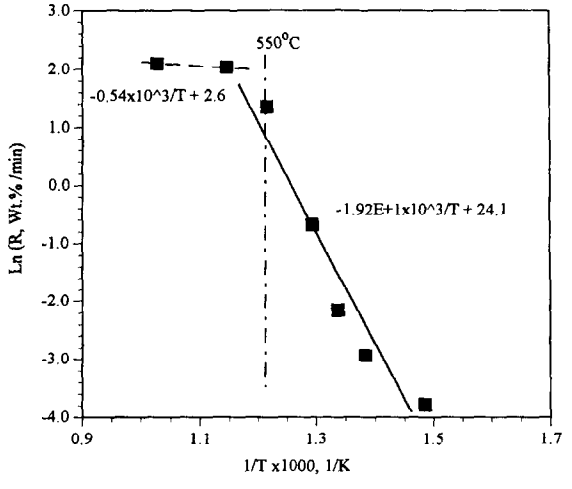

Fig. 11. Arrhenius plot of initial reduction rate of sulfated catalyst.

4. Conclusions

The catalytic performance of fluorite oxides and transition metal/fluorite oxide composite materials for SO_2 reduction by CO can be well explained within the redox framework. Generation of the oxygen vacancy is a key step to initiate the reaction. The oxygen vacancy property of fluorite oxide is important for redox catalysis. The transition metal/fluorite oxide composite is a class of highly active and stable catalysts for SO_2 reduction by CO to elemental sulfur through a synergistic effect. For Cu–Ce–O system, the stable cerium oxide serves as the backbone of the catalyst structure and as the oxygen vacancy source, while copper promotes the reducibility of the cerium oxide and provides surface sites for CO adsorption. SO_2 has a strong affinity to cerium oxide such that a working Cu–Ce–O catalyst comprises partially reduced and partially sulfated cerium oxide.

The reduction studies of the Cu–Ce–O catalyst by H_2 and CO have demonstrated a 'strong interaction' of copper and cerium oxide that resembles that of the precious metal/CeO_2 systems. The surface oxygen of the Cu–Ce–O composite is highly active but its reactivity is severely inhibited by SO_2 adsorption.

Acknowledgements

This work was supported by the U.S. Department of Energy, University Coal research Program, under Grant DE-FG22-92PC92534. The authors would like to thank Dr. A. Tschope and Prof. J.Y. Ying for the synthesis of the non-

stoichiometric cerium oxide catalysts and Dr. C.W. Krueger for his assistance with the TGA/MS study. This work made use of the MRSEC Shared Facilities supported by the National Science Foundation under Award DMR-P400334.

References

[1] J.M. Whelan, US Pat. 4,081,519 (1978).
[2] J. Happel, M.A. Hnatow, L. Bajars and M. Kundrath, Ind. Eng. Chem., Prod. Res. Dev., 14 No.3 (1975) 154.
[3] J. Happel, A.L. Leon, M.A. Hnatow and L. Bajars, Ind. Eng. Chem., Prod. Res. Dev., 16 No.2 (1977) 150.
[4] D.B. Hibbert and R.H. Campbell, Appl. Catal., 41 (1988) 273.
[5] D.B. Hibbert and R.H. Campbell, Appl. Catal., 41 (1988) 289.
[6] N.Q. Minh, J. Am. Ceram. Soc., 76(3) (1993) 563.
[7] J.A. Baglio, Ind. Eng. Chem. Prod. Res. Dev., 21 (1982) 38.
[8] M. Flytzani-Stephanopoulos and Z. Hu, US Pat. 5,242,673 (1993).
[9] W. Liu and M. Flytzani-Stephanopoulos, in J.N. Armor (Editor), Environmental Catalysis (ACS Symposium Series 552), American Chemical Society, Washington, DC, 1994, p.375.
[10] M. Flytzani-Stephanopoulos and W. Liu, US Pat. 5,384,301 (1995).
[11] W. Liu, A.F. Sarofim and M. Flytzani-Stephanopoulos, Appl. Catal. B, 4 (1994) 167.
[12] P. Hagenmuller and W. van Gool, Solid Electrolytes, Academic Press, New York, 1978.
[13] A. Tschöpe and J.Y. Ying, J. Nanostr. Mater., 4 [5] (1994) 617.
[14] A. Tschöpe, W. Liu, M. Flytzani-Stephanopoulos and J.Y. Ying, J. Catal., 157 (1995) 42.
[15] D.J. Kim, J. Am. Ceram. Soc., 72(8) (1989) 1415.
[16] Stud. Surf. Sci. Catal., 71 (1991).
[17] V. Butler, C.R.A. Catlow, B.E.F. Fender and J.H. Harding, Solid State Ionics, 8 (1983) 109.
[18] C. Li, Y. Sakata, T. Arai, K. Domen, K. Maruya and T. Onishi, J. Chem. Soc., Faraday Trans. 1, 85 (1989) 929.
[19] C. Li, Y. Sakata, T. Arai, K. Domen, K. Maruya and Onishi, J. Chem. Soc., Faraday Trans. 1, 85 (1989) 1451.
[20] P.R. Ryason and J. Harkins, J. Air Pollut. Contr. Ass., 17 (1967) 796.
[21] L.A. Haas and S.E. Khalafalla, J. Catal., 30 (1973) 451.
[22] J.G.L. Bazes, L.S. Careto and K. Noble, Ind. Eng. Chem., Prod. Res. Develop., 14 (1975) 264.
[23] W. Liu, Sc.D. Thesis, Massachusetts Institute of Technology, May 1995.
[24] W. Liu and M. Flytzani-Stephanopoulos, J. Catal., 153 (1995) 304.
[25] W. Liu and M. Flytzani-Stephanopoulos, J. Catal., 153 (1995) 317.
[26] M.B. Badley, C.H. Rochester, G.J. Hutchings and F. King, J. Catal., 148 (1994) 438.
[27] H.C. Yao and Y.F.Y. Yao, J. Catal., 86 (1984) 254.
[28] G. Fierro, M.L. Jacono, M. Inversi, P. Porta, R. Lavecchia and F. Cioci, J. Catal., 148 (1994)709.
[29] A.L. Boyce, S.R. Graville, P.A. Sermon and M.S.W. Vong, React. Kinet. Catal. Lett., 434(1) (1991) 1.
[30] J.G. Nunan, R.G. Silver and S.A. Bradley, in R.G. Silver, J.E. Sawyer and J.C. Summers (Editors), Catalytic Control of Air Pollution (ACS Symposium Series 495), American Chemical Society, Washington, DC, 1992, p.83.
[31] S.W. Hedges and J.T. Yeh, Environmental Progress, 11(2) (1992) 98.